Acta Cryst C STRUCTURAL CHEMISTRY

ISSN 2053-2296

Molecular structure and selective theophylline complexation by conformational change of diethyl *N*,*N*′-(1,3-phenylene)dicarbamate

Juan Saulo González-González,[a]* Alfonso Martínez-Santos,[a] María José Emparán-Legaspi,[b] Armando Pineda-Contreras,[b] Francisco Javier Martínez-Martínez,[b] Marcos Flores-Alamo[c] and Hector García-Ortega[c]*

[a]Instituto de Farmacobiología, Universidad de la Cañada, Carretera Teotitlán-San Antonio Nanahuatipán, km 1.7 s/n, Teotitlán de Flores Magón, Oaxaca 68540, Mexico, [b]Facultad de Ciencias Químicas, Universidad de Colima, km 9, Carretera Colima-Coquimatlán, Coquimatlán, Colima 28400, Mexico, and [c]Facultad de Química, Universidad Nacional Autónoma de México, Ciudad de México 04510, Mexico. *Correspondence e-mail: juan_saulo@unca.edu.mx, hector.garcia@unam.mx

Received 21 March 2024
Accepted 16 April 2024

Edited by M. Rosales-Hoz, Cinvestav, Mexico

Keywords: mechanochemistry; crystal structure; host-guest complex; phenyl carbamate; conformational change; IR spectroscopy; theophylline.

CCDC references: 2328711; 2328710

Supporting information: this article has supporting information at journals.iucr.org/c

The receptor ability of diethyl *N*,*N*′-(1,3-phenylene)dicarbamate (**1**) to form host–guest complexes with theophylline (TEO) and caffeine (CAF) by mechanochemistry was evaluated. The formation of the **1**–TEO complex ($C_{12}H_{16}N_2O_4{\cdot}C_7H_8N_4O_2$) was preferred and involves the conformational change of one of the ethyl carbamate groups of **1** from the *endo* conformation to the *exo* conformation to allow the formation of intermolecular interactions. The formation of an N—H···O═C hydrogen bond between **1** and TEO triggers the conformational change of **1**. CAF molecules are unable to form an N—H···O═C hydrogen bond with **1**, making the conformational change and, therefore, the formation of the complex impossible. Conformational change and selective binding were monitored by IR spectroscopy, solid-state ^{13}C nuclear magnetic resonance and single-crystal X-ray diffraction. The **1**–TEO complex was characterized by IR spectroscopy, solid-state ^{13}C nuclear magnetic resonance, powder X-ray diffraction and single-crystal X-ray diffraction.

1. Introduction

Host–guest complexes are supramolecular species formed by two or more molecules or ions stabilized by noncovalent interactions (principally hydrogen bonds) involving molecular recognition between the functional groups of both. A host (or receptor) is a molecule with a cavity suitable for guest binding. The design of molecular receptors involves an understanding of the intermolecular interactions using building blocks with functional groups that allow the binding of specific guests (or substrates). The study of host–guest complexes in solution and the solid state has allowed its application in various fields, such as drug delivery systems (Wankar *et al.*, 2020), molecular diagnostics (Yu & Chen, 2019), biomaterials (Webber *et al.*, 2016), artificial molecular machines (Erbas-Cakmak *et al.*, 2015), sensors (Kim *et al.*, 2012) and biosensors (Lim *et al.*, 2021).

Molecules with the amide group [*R*′–NH–(C═O)–*R*] have been used in the design of molecular receptors due to their ability to act as a donor and acceptor of hydrogen bonds in the formation of supramolecular complexes. These amide receptors have been exploited in a cyclic and acyclic manner using functionalities such as carboxamides (Bondy & Loeb, 2003), ureas (dos Santos *et al.*, 2008), oxalamates (González-González *et al.*, 2014), amino acids (Kubik & Mungalpara, 2017) and carbamates (Saucedo-Balderas *et al.*, 2015), which have been studied in the formation of supramolecular complexes

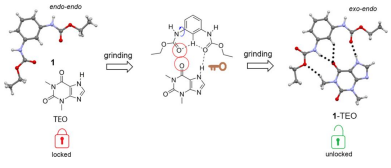

with anions, polyphenols, amino acids and pharmaceutical ingredients (Siering *et al.*, 2006).

Phenyl carbamate is an organic group used in drug design with biological applications, such as acetylcholinesterase inhibitors for the treatment of Alzheimer's disease (Colović *et al.*, 2013; Krátký *et al.*, 2016), antiparasitic agents (Angeles *et al.*, 2000; Jiménez-Cardoso *et al.*, 2004) and anticonvulsants (Matošević & Bosak, 2020). In organic synthesis they are used as precursors of isocyanates (Baba *et al.*, 2005; Sun *et al.*, 2013) and in the chiral separation of antifungal agents (Ali *et al.*, 2021).

The chemical structure of phenyl carbamates includes carbonyl (C═O) and amino (N—H) groups, which can form inter- and intramolecular hydrogen-bond interactions. Also π-interactions can be formed by the phenyl ring (Matošević & Bosak, 2020). Supramolecular studies of phenyl carbamates (Shahwar *et al.*, 2009; AaminaNaaz *et al.*, 2017) are focused on the self-assembly of crystal structures, revealing that the N—H···O═C hydrogen-bond interaction drives the supramolecular architecture in the solid state, leading to the formation of supramolecular chains in phenyl carbamate derivatives, and supramolecular columns in phenylenebis-carbamates (García-Báez *et al.*, 2004; Lu *et al.*, 2005*a*,*b*).

Theophylline (bronchodilator) and caffeine (nervous system stimulant) are pharmacologically active molecules (Boushey, 2012) that possess functional groups (C═O and N—H in only TEO) capable of forming noncovalent interactions which have been applied in the development of molecular receptors for the molecular recognition of TEO and CAF due to its potential biomedical and industrial applications (Sahoo, 2015).

The formation of supramolecular complexes has allowed the identification and quantification of compounds of pharmaceutical interest. To evaluate the ability of diethyl *N*,*N*′-(1,3-phenylene)dicarbamate (**1**) as a receptor to form host–guest complexes, we report here the mechanochemical complexation of **1** with theophylline (TEO) and caffeine (CAF) (Scheme 1). The obtained **1**–TEO complex was prepared by solvent-assisted grinding and was characterized by IR spectroscopy (IR), powder X-ray diffraction (PXRD) and solid-state ^{13}C nuclear magnetic resonance (NMR). The molecular structure was obtained by single-crystal X-ray diffraction.

2. Experimental

2.1. compounds

1,3-Phenylenediamine, ethyl chloroformate, triethylamine, tetrahydrofuran (THF) anhydrous, dimethyl sulfoxide (DMSO) anhydrous and theophylline anhydrous were purchased from Aldrich. Chloroform, dichloromethane, methanol and acetonitrile of ACS grade were purchased from Química Mayer. Caffeine was purchased from BASF. All the reagents were used as received.

2.2. Synthesis of diethyl *N*,*N*′-(1,3-phenylene)dicarbamate, 1

A mixture of 1,3-phenylenediamine (3.0 g, 27.7 mmol) and triethylamine (61.0 mmol, 8.5 ml) in tetrahydrofuran (THF, 250 ml) was placed in an ice bath. After 10 min of stirring, ethyl chloroformate (5.3 ml, 61.0 mmol) was added dropwise. The mixture was stirred for 24 h at room temperature and then filtered to obtain a THF solution which was evaporated to dryness. The obtained solid was solubilized in chloroform and filtered to separate the insoluble solid. The chloroform solution was evaporated to obtain a solid corresponding to compound **1**.

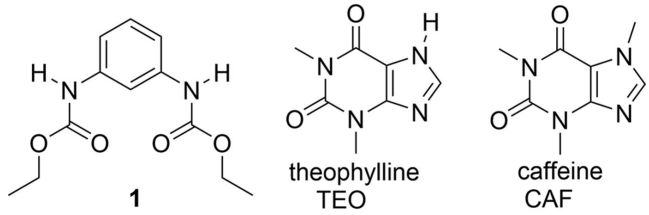

Scheme 1

Analytical data for **1**: yield 53.17%; white solid; m.p. 146–148 °C; IR (ATR): ν (cm^{-1}) 3283 (N—H), 1704, 1688 (C═O). ^{1}H NMR (DMSO-d_6, 400 MHz, δ ppm): 9.55 (*s*, 2H, N–H7), 7.70 (*s*, 1H, H2), 7.07 (*dd*, 2H, J = 7.0, 2.2 Hz, H4, H6), 7.13 (*t*, 1H, J = 6.9 Hz, H5). ^{13}C NMR (DMSO-d_6, 100 MHz, δ ppm): 153.9 (C8), 140.0 (C1, C3), 129.1 (C2), 113.1 (C4, C6), 60.4 (C10), 14.9 (C11). Analysis calculated (%) for $C_{12}H_{16}N_2O_4$: C 57.13, H 6.93, N 11.10; found: C 56.82, H 6.39, N 11.04.

2.3. Mechanochemical synthesis and crystallization

A mixture in a 1:1 molar ratio of **1** (0.30 g, 1.18 mmol) and TEO (0.21 g, 1.18 mmol) was placed in a porcelain mortar. Before starting the grinding with a pestle, 0.5 ml of dichloromethane was added and the mixture was ground for 3 min. At the end of the grinding time, the dichloromethane was evaporated and the ground powder was collected in the centre of the mortar. The cycle of adding 0.5 ml of dichloromethane and grinding for 3 min was repeated three more times until 12 min of grinding time was completed. After 12 min of grinding time, the obtained ground powder was stored in a glass vial. **1**–CAF ground powder was obtained by grinding **1** (0.30 g, 1.18 mmol) and CAF (0.22 g, 1.18 mmol) under the same conditions as described for the **1**–TEO mixture.

Solutions of **1** and **1**–TEO were prepared by dissolving the powder of **1** in DMSO and the ground powder of **1**–TEO in a 1:1 methanol/acetonitrile mixture. Single crystals were obtained after evaporation of the solvent.

2.4. Instrumentation

The IR spectra of solids **1**, TEO, **1**–TEO ground powder, **1**–TEO single crystal, CAF and **1**–CAF ground powder were obtained in a Bruker Tensor-27 spectrophotometer equipped with an attenuated total reflectance (ATR) system (16 scans, spectral range 600–4000 cm^{-1}, resolution 4 cm^{-1}).

Powder X-ray diffraction patterns of solids **1**, TEO, polycrystalline **1**–TEO ground powder, CAF and **1**–CAF polycrystalline ground powder were collected on a PANalytical

Table 1
Experimental details.

Experiments were carried out with Mo $K\alpha$ radiation using a Agilent Xcalibur Atlas Gemini diffractometer. The absorption correction was analytical (*CrysAlis PRO*; Agilent, 2013). H atoms were treated by a mixture of independent and constrained refinement.

	1	**1**–TEO
Crystal data		
Chemical formula	$C_{12}H_{16}N_2O_4$	$C_{12}H_{16}N_2O_4{\cdot}C_7H_8N_4O_2$
M_r	252.27	432.44
Crystal system, space group	Tetragonal, $P4_12_12$	Triclinic, $P\bar{1}$
Temperature (K)	298	130
a, b, c (Å)	11.1312 (13), 11.1312 (13), 10.894 (3)	7.5284 (14), 11.2362 (18), 12.2606 (12)
α, β, γ (°)	90, 90, 90	85.742 (10), 76.887 (12), 79.803 (15)
V (Å^3)	1349.8 (5)	993.5 (3)
Z	4	2
μ (mm^{-1})	0.09	0.11
Crystal size (mm)	0.41 × 0.33 × 0.3	0.38 × 0.12 × 0.07
Data collection		
T_{min}, T_{max}	0.972, 0.976	0.976, 0.993
No. of measured, independent and observed [$I > 2\sigma(I)$] reflections	4765, 1620, 1153	11140, 4780, 3041
R_{int}	0.027	0.051
$(\sin \theta/\lambda)_{max}$ (Å^{-1})	0.693	0.697
Refinement		
$R[F^2 > 2\sigma(F^2)]$, $wR(F^2)$, S	0.047, 0.128, 1.05	0.062, 0.157, 1.05
No. of reflections	1620	4780
No. of parameters	87	290
$\Delta\rho_{max}$, $\Delta\rho_{min}$ (e Å^{-3})	0.12, −0.14	0.29, −0.38
Absolute structure	Flack x determined using 343 quotients $[(I^+) - (I^-)]/[(I^+) + (I^-)]$ (Parsons *et al.*, 2013)	–
Absolute structure parameter	−1.9 (9)	–

Computer programs: *CrysAlis PRO* (Agilent, 2013), *SHELXT2018* (Sheldrick, 2015*a*), *SHELXL2018* (Sheldrick, 2015*b*), *ORTEP-3 for Windows* (Farrugia, 2012) and *WinGX* (Farrugia, 2012).

X′pert Pro diffractometer with Cu $K\alpha_1$ radiation (λ = 1.5405 Å, 45 kV, 40 mA) from 5.0 to 50.0° in 2θ.

Solution ^{1}H and ^{13}C NMR spectra of **1** were recorded on a Bruker 400 Avance III spectrometer (^{1}H = 400 MHz and ^{13}C = 100 MHz) at room temperature (25 °C) using DMSO-d_6 as solvent and $SiMe_4$ as the internal reference (the NMR spectra of **1** are shown in Figs. S1 and S2 in the supporting information). Solid-state cross-polarization/magic angle spinning (CP/MAS) ^{13}C spectra of **1**, TEO and the polycrystalline ground powder of **1**–TEO were recorded on a Bruker 400 Avance III (^{13}C = 100 MHz) instrument at 25 °C, using 4 mm bullet-type Kel-F zirconia rotors with a spinning rate of 8 kHz and an acquisition time of 32 ms. The recycle time of the pulse was 3 s. An adamantane signal was used as the external reference (δ = 38.48 ppm). Processing of the NMR spectra was performed with *MestReNova* software (Version 14.2.0-26256; Mestrelab Research, 2021).

Elemental analysis of **1** was performed using a vario MICRO Cube CHN(S) analyzer (Fig. S3 in the supporting information).

The melting point (m.p.) of **1** was measured using an Electrothermal IA9300 apparatus and is uncorrected.

2.5. Refinement

Crystal data, data collection and structure refinement details are summarized in Table 1. The H atoms of the amine group (H—N) were located in a difference map and refined isotropically with $U_{iso}(H) = 1.2U_{eq}(N)$ for H—N hydrogens. H atoms attached to C atoms were placed in geometrically idealized positions and refined as riding on their parent atoms, with C—H = 0.93–0.99 Å and $U_{iso}(H) = 1.2U_{eq}(C)$ for aromatic and methylene groups, and $1.5U_{eq}(C)$ for methyl groups.

Table 2
IR frequencies (cm^{-1}).

Compound	N—H	ΔN—H	C═O	ΔC═O
1	3283	–	1704, 1688	–
TEO	3120	–	1705, 1662	–
1–TEO$_{ground}$	3312, 3293, (3169)	29, 10, (49)	1700, (1638)	(−5), 12, −4*, (−24)
1–TEO$_{cryst}$	3309, 3292, (3162)	26, 9, (42)	1698, (1638)	(−7), 10, −6, (−24)
CAF	–	–	1694, 1645	–
1–CAF$_{ground}$	3284	1*	1705, 1692, (1658)	1*, 4*, (13)**

Notes: (*) under spectral resolution; (**) the apparent shift of the band is due the change of the curvedness of the C═O band in the IR spectra. Values in brackets belong to the IR frequencies of TEO or CAF.

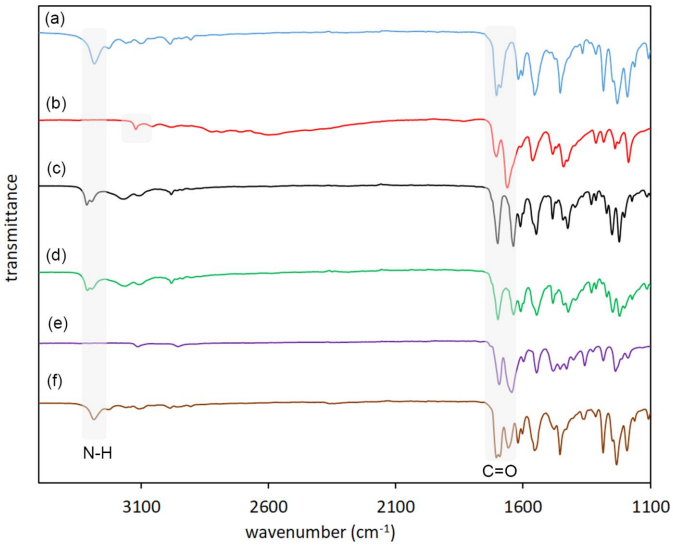

Figure 1
The IR spectra of (*a*) **1**, (*b*) TEO, (*c*) the polycrystalline powder of **1**–TEO after 12 min of grinding, (*d*) a single crystal of **1**–TEO, (*e*) CAF and (*f*) the ground powder of **1**–CAF.

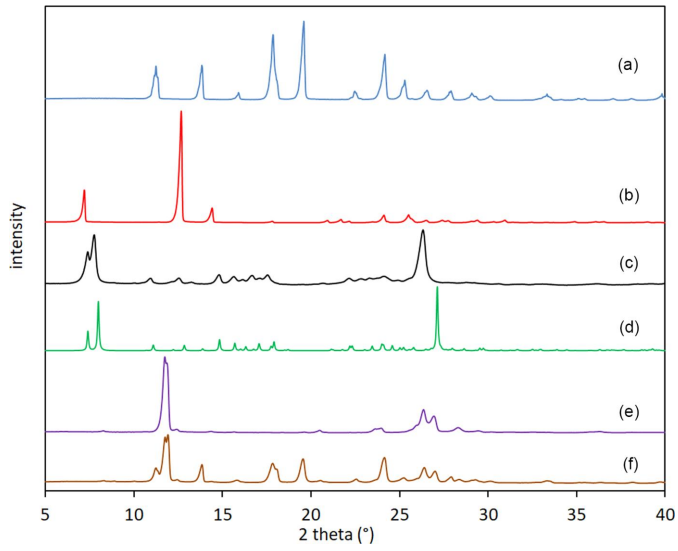

Figure 3
The powder X-ray diffractograms of (*a*) **1**, (*b*) TEO, (*c*) **1**–TEO ground powder, (*d*) the simulated pattern of **1**–TEO, (*e*) CAF and (*f*) **1**–CAF ground powder.

3. Results and discussion

3.1. IR spectroscopy

The IR spectra of **1**, TEO and CAF (González-González *et al.*, 2017) were compared with the IR spectra of the polycrystalline ground powders (**1**–TEO and **1**–CAF) and the single crystal of **1**–TEO (the IR frequencies are listed in Table 2). The formation of the **1**–TEO powder complex was evidenced by the shift of the N—H and C═O stretching bands in the IR spectrum of the **1**–TEO ground powder with respect to the starting compounds, suggesting the formation of intermolecular N—H···O═C hydrogen bonds (Fig. 1). On the other hand, the IR spectrum of the **1**–CAF ground powder did not show shifts with respect to the starting materials, suggesting that the formation of the **1**–CAF complex was not favored under mechanochemical conditions.

The IR spectrum of the **1**–TEO powder complex and the IR spectrum of the single crystal were similar, indicating a structural homogeneity between the powder and the single crystal. The IR spectrum of **1** showed a single N—H band at 3283 cm^{-1}. After the formation of the complex, the N—H band was red-shifted and split (suggesting asymmetry in the molecule) into two bands with values of 3312 and 3293 cm^{-1} [$\Delta\nu$(N—H) = 10 and 29 cm^{-1}, respectively]. The N—H band of TEO was also red-shifted as a consequence of the complex formation from 3120 to 3169 cm^{-1} [$\Delta\nu$(N—H) = 49 cm^{-1}].

Concerning the carbonyl frequencies, compound **1** showed two bands at 1704 and 1688 cm^{-1}, with $\Delta\nu$(C═O) = 12 and −4 cm^{-1}. Theophylline showed $\Delta\nu$(C═O) = −5 and −24 cm^{-1}.

The grinding process reorders the hydrogen-bonding patterns of the compounds involved in the formation of the complex shifting the C═O and N—H bands. Compound **1** is self-assembled by N—H···O═C hydrogen bonds [*C*(4) homosynthon] in the free form (see *Single-crystal X-ray diffraction*, §3.4). After the formation of the **1**–TEO complex, the N—H···O═C hydrogen-bond (heterosynthon) pattern is maintained; this explains the smaller values of $\Delta\nu$(N—H) and $\Delta\nu$(C═O) compared with the starting **1**. On the other hand, in the free form of TEO, the molecules are interlinked by N—H···N(imidazole) hydrogen bonds and π-interactions (Larkin *et al.*, 2014) (Fig. 2). The rearrangement of these hydrogen-bond patterns to form a new hydrogen-bond pattern results in greater $\Delta\nu$(N—H) and $\Delta\nu$(C═O) values of TEO with respect to the $\Delta\nu$(N—H) and $\Delta\nu$(C═O) values of **1**.

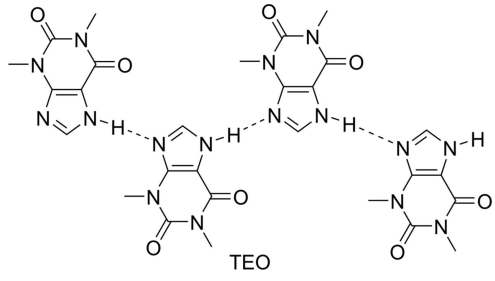

Figure 2
Hydrogen-bond patterns in free TEO.

3.2. Powder X-ray diffraction

The powder X-ray diffraction patterns of the polycrystalline powder of **1**, solid TEO and CAF, and the polycrystalline powder of **1**–TEO and **1**–CAF were obtained. The solid form of TEO and CAF were identified as form II (Liu *et al.*, 2013; Mazel *et al.*, 2011) of each compound from the experimental powder diffraction pattern. The recorded powder pattern of **1** was similar to that simulated with *Mercury* (Macrae *et al.*, 2020) (Fig. S4), indicating structural homogeneity between the polycrystalline powder and the single crystal. The formation of the polycrystalline complex was evidenced because the PXRD

Table 3
Solid-state ^{13}C chemical shifts of **1**, TEO and **1**–TEO (δ = ppm).

	C1,C3	C2	C4,C6	C8	C9	C10	C*a*	C*b*	C*c*	C*d*	C*e*	C*f,g*
1	140.1	130.4	114.6	155.9	61.2	12.8	–	–	–	–	–	–
TEO	–	–	–	–	–	–	154.9	105.8	140.5	146.3	150.9	30.0
1–TEO	140.7	129.9	111.9, 110.3	154.5	64.1, 62.4	12.6, 11.6	154.5	106.8	140.7	147.6	151.9	29.9

diffraction pattern of the **1**–TEO polycrystalline ground powder was different compared with those of the starting materials (Fig. 3), showing new diffraction peaks at 2θ = 7.7, 14.8, 16.7 and 23.4°, and was similar to that simulated with *Mercury* (Macrae *et al.*, 2020). The absence of the signals at 2θ = 19.6 and 12.5° of starting **1** and TEO, respectively, in the powder pattern of **1**–TEO indicates the complete transformation of **1** and TEO to form the complex (Fig. 3). The PXRD pattern of **1**–CAF showed a combined pattern of **1** and CAF as a physical mixture [Fig. 3(*f*)] thus showing that the **1**–CAF complex was not formed.

3.3. Solid-state ^{13}C NMR

The solid-state ^{13}C NMR spectra of **1**, TEO and the **1**–TEO powder complex were recorded (Fig. 4) and the ^{13}C NMR assignments are listed in Table 3. Most of the signals in the ^{13}C NMR spectrum of the **1**–TEO complex appeared shifted with respect to the starting compounds as a result of the change in the chemical environment due to the rearrangement of the hydrogen-bond patterns. The C═O signals were shifted from 155.9 to 154.5 ppm in **1** and from 150.9 to 151.9 ppm in TEO, indicating the formation of C═O···H—N hydrogen bonds between **1** and TEO. It worthy of mention that in the solid-state ^{13}C NMR spectrum of **1**, only half of the signals were observed, indicating the presence of a C_2 symmetry axis, which is consistent with the *endo–endo* conformation of **1**, as confirmed by single-crystal diffraction. Meanwhile, in the solid-state ^{13}C NMR spectrum of the **1**–TEO complex, the signals of C10 and C11 from the ethyl group, and also the aromatic C4 and C6 signals, appeared split (Table 3), suggesting two crystallographically different ethyl groups originated from the adoption of the *exo–endo* conformation after the formation of the **1**–TEO complex.

3.4. Single-crystal X-ray diffraction

The carbamate group in phenyl carbamates can adopt the *syn* or *anti* conformation according to the H7—N7—C8—O8 torsion angle [Fig. 5(*a*)]. A search of crystal structures in the Cambridge Structural Database (CSD, Version 5.45, update of November 2023; Groom *et al.* 2016) under the 'phenylcarbamate' criteria, showed 98 results where the carbamate group adopts the *anti* conformation, and only one where the carbamate group adopts the *syn* conformation, *i.e.* the crystal structure of diisopropyl *N*,*N*′-(4-methyl-*m*-phenylene)dicarbamate (CSD refcode JAYBUH; Lu *et al.*, 2005*b*). Taking into consideration the cavity formed by the ethyl carbamate groups with respect to the benzene ring (torsion angle C6—C1—N7—C8), compound **1** can adopt the *endo–endo*, *exo–endo* and *exo–exo* conformations [Fig. 5(*b*)]. Four examples of crystal structures of 1,3-phenylenedicarbamates have been reported (Fig. S5): two adopt the *endo–endo* conformation [refcodes GAVGEQ (Lu *et al.*, 2005*a*) and JAYBUH (Lu *et al.*,

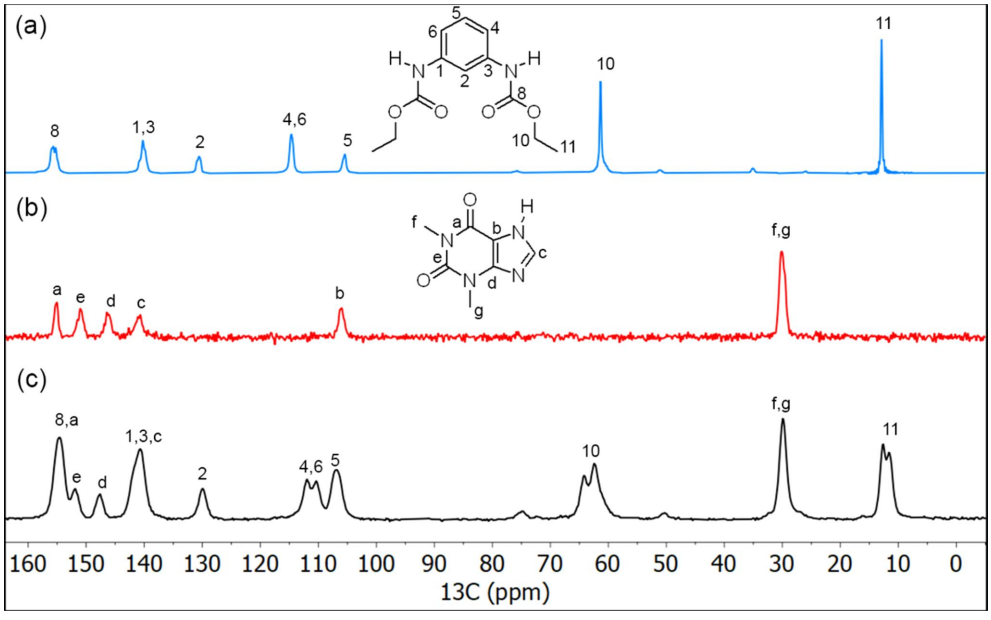

Figure 4
^{13}C NMR spectra of (*a*) **1**, (*b*) TEO and (*c*) the **1**–TEO complex.

Table 4
Hydrogen-bond geometry (Å, °) for **1** and **1**–TEO.

	D—H···A	D—H	H···A	D···A	D—H···A
1	N7—H7···O8^{i}	0.93 (3)	1.97 (3)	2.897 (3)	176 (3)
	C6—H6···O8	0.93	2.38	2.950 (3)	119
	C6—H6···O8^{ii}	0.93	2.38	2.950 (3)	119
1–TEO	N7—H7···O6^{iii}	0.91 (3)	2.02 (3)	2.920 (3)	168 (2)
	N7—H7C···O10^{iii}	0.88	1.90	2.770 (3)	172
	N27—H27···O2C^{iv}	0.94 (2)	1.96 (2)	2.877 (2)	167 (2)
	C2—H2C···O6C^{iii}	0.95	2.52	3.306 (3)	140
	C1C—H1CB···O9^{iii}	0.98	2.49	3.399 (3)	153
	C4—H4C···O2C^{iv}	0.95	2.44	3.219 (3)	139
	C8—H8C···O8^{v}	0.95	2.48	3.303 (3)	145
	C1C—H1CC···O10^{vi}	0.98	2.57	3.400 (3)	142
	C2—H2···O10	0.95	2.23	2.849 (3)	122
	C6—H6···O8	0.95	2.29	2.895 (3)	121

Symmetry codes: (i) $y+\frac{1}{2}, -x+\frac{1}{2}, z-\frac{1}{4}$; (ii) $y, x, -z+1$: (iii) $-x+1, -y+1, -z+1$; (iv) $-x+1, -y+1, -z$; (v) $-x, -y+2, -z+1$; (vi) x, y, z.

2005*b*)] and two adopt the *exo–exo* conformation [refcodes PIRQUG (Piper *et al.*, 2023) and OWOYIL (Alegre-Requena *et al.*, 2020)].

Compound **1** crystallized in the tetragonal space group $P4_12_12$, with the molecule lying across a twofold axis having C_2 symmetry; thus, only one half of the molecule is present in the asymmetric unit. The crystal structure of **1** [Fig. 6 (*a*)] adopts the *endo–endo* conformation [with the C6—C1—N7—C8 torsion angle = −14.5 (4)°], reinforced by the formation of the C═O···H···O═C three-centred intramolecular hydrogen bonds (C6—H6···O8 = 2.38 Å), depicting two adjacent $S(6)$ motifs (the hydrogen-bond details and symmetry codes for **1** are given in Table 4). The ethyl carbamate group is twisted out from the plane of the benzene ring by 2.2 (4)° (C1—N7—C8—O8 torsion angle). The carbamate group adopts the *anti* conformation, with the H7—N7—C8—O8 torsion angle being 175.6 (2)°. Each molecule of **1** is linked with four molecules by N7—H7···O8 (1.97 Å) hydrogen bonding. This interaction is extended along the *ab* plane to form a bidimensional supramolecular arrangement depicting $C(4)$ hydrogen-bond motifs [Fig. 6 (*b*)], as observed in GAVGEQ (Lu *et al.*, 2005*a*), JAYBUH (Lu *et al.*, 2005*b*) and PIRQUG (Piper *et al.*, 2023).

The **1**–TEO complex crystallized in the triclinic space group $P\overline{1}$, the discrete unit consist of one molecule of **1** and one molecule of TEO [Fig. 7 (*a*)]. Receptor **1** adopts the *exo–endo* conformation, with torsion angles C2—C1—N7—C8 = 175.6 (2)° and C2—C3—N27—C28 = 2.8 (4)°, and the carbonyl group adopts the *syn* conformation, with torsion angles H7—N7—C8—O8 = 177.6 (2)° and H27—N27—C28—O10 = 177.9 (2)°.

The pseudoamide fragment of the TEO molecule (O6C—C6C—C5C—N7C—H7C) is involved in the formation of TEO cocrystals with amidic coformers (Eddleston *et al.*,

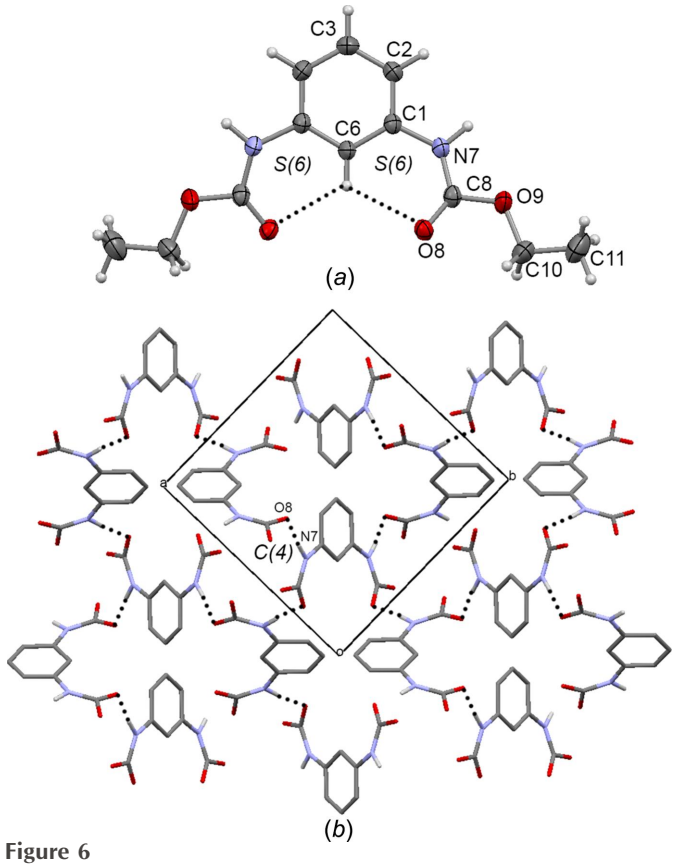

Figure 6
(*a*) The molecular structure of **1**, with displacement ellipsoids drawn at the 30% probability level, showing the intermolecular interactions. (*b*) The supramolecular arrangement of **1** formed by N—H···O═C hydrogen bonds. Dashed lines represent hydrogen bonds. Some parts of the molecules have been omitted for clarity. Dashed lines represent hydrogen bonds.

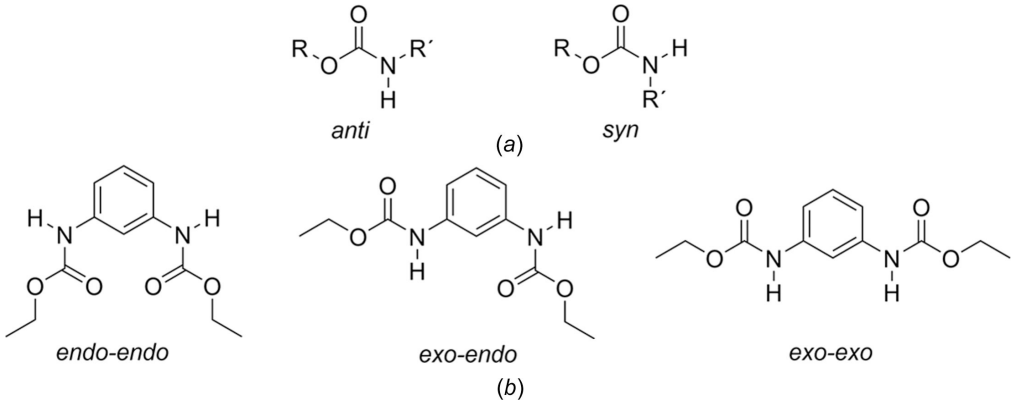

Figure 5
(*a*) Possible conformations of the carbamate group and (*b*) possible conformations of **1**.

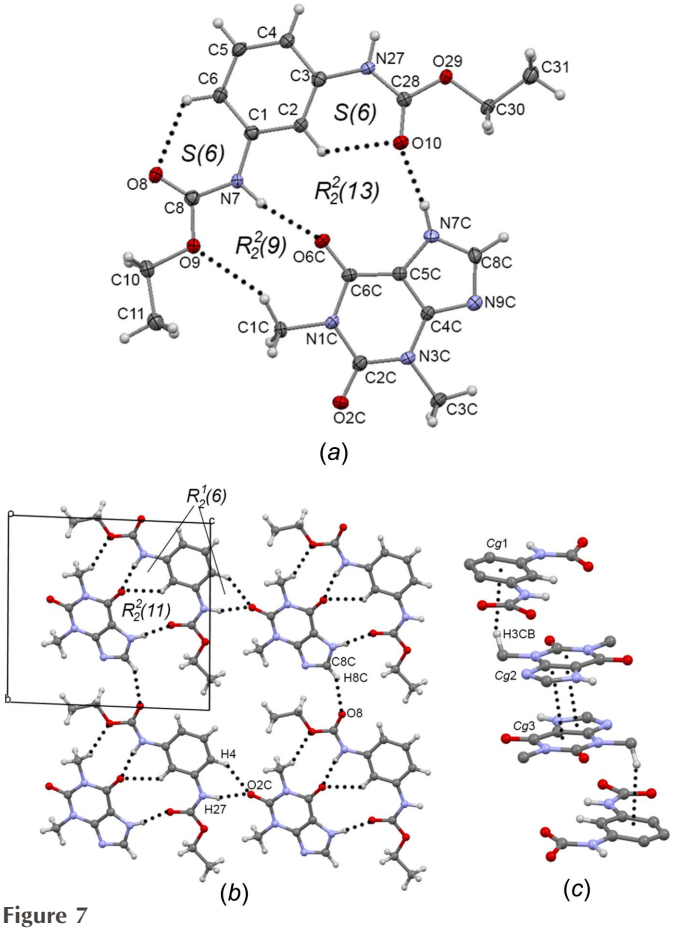

Figure 7
(*a*) The asymmetric unit, with displacement ellipsoids at the 30% probability level, of **1**–TEO, showing the atom numbering. (*b*) The supramolecular sheet of **1**–TEO formed by the N27—H27···O2*C*^{iv} and C8*C*—H8*C*···O8^{v} interactions. (*c*) π–π and C—H···π interactions found in **1**–TEO. Some parts of the molecules have been omitted for clarity. Dashed lines represent hydrogen bonds or noncovalent interactions.

2016; Markad & Mandal, 2017). When the coformer is a primary or secondary amide group, the $R_2^2(9)$ amide-pseudoamide synthon is formed [Fig. 8(*a*)], meanwhile the $R_2^2(10)$ pseudoamide–pseudoamide synthon consists of the self-assembly of two TEO molecules [Fig. 8(*b*)], where the coformer is hydrogen bonded to TEO by the the urea carbonyl or the imidazole N atom. Receptor **1** and TEO are interlinked by intermolecular N—H···O═C hydrogen bonds [N7—H7···O6*C* = 2.02 (3) Å and N7*C*—H7*C*···O10 = 1.90 Å] depicting a new synthon, *i.e.* the $R_2^2(13)$ 'diamide–pseudoamide' synthon [Fig. 8(*c*)] [this motif can be fragmented in two adjacent $R_2^1(6)$ and $R_2^2(11)$ motifs, including the C2—H2···O6*C* interaction] [Fig. 7(*b*)]. The complementary C1*C*—H1*CB*···O9 (2.49 Å) interaction, depicting an $R_2^2(11)$ motif, is also involved in the interconnection of **1** and TEO. The angle between the planes formed by the benzene ring and the TEO molecule is 9.42°, indicating that **1** and TEO are almost coplanar and the good fit of TEO into the cavity formed by the ethyl carbamate groups. The intramolecular C2—H2···O10 *S*(6) interaction becomes shorter (2.22 Å) compared with starting **1** (2.38 Å). The observed intermolecular interactions between **1**–TEO units, *i.e.* the N27—H27···O2*C* = 1.96 (2) Å hydrogen bond, and the C4—H4···O2*C* = 2.44 Å [$R_2^1(6)$ motif] and C8—H8*C*···O8*C* = 2.48 Å interactions, give rise to a bidimensional supramolecular sheet extended along the *bc* plane [Fig. 7(*b*)]. Supramolecular sheets are connected by π-stacking of TEO (*Cg*2···*Cg*3 = 3.35 Å; *Cg*2 and *Cg*3 are the centroids of the N7*C*/C5*C*/C4*C*/N9*C*/C8*C* and N1*C*/C2*C*/N3*C*/C4*C*/C5*C*/C6*C* rings, respectively) and C—H···π interactions (C3—H3*CB*···*Cg*1 = 2.87 Å; *Cg*1 is the centroid of the C1/C2/C3/C4/C5/C6 ring) [Fig. 7(*c*)].

3.5. Conformational change of 1 and selective binding of TEO

The molecular structure of starting **1** adopts the *endo–endo* conformation, showing a single N—H band in the IR spectrum and half of the signals in the solid-state ^{13}C NMR spectrum. The formation of the **1**–TEO complex by mechanochemical grinding involves the conformational change of **1** from the *endo–endo* conformation to the *exo–endo* conformation (showing two N—H bands in the IR spectrum and the split of the ethyl signals in the solid-state ^{13}C NMR spectrum of **1**–TEO), while the grinding of **1** and CAF under the same conditions used to obtain **1**–TEO did not result in the formation of the **1**–CAF complex.

In the *endo–endo* conformation, a potential carbonyl–carbonyl repulsive effect avoids the complex formation by adopting a 'locked' state (Fig. 9). The formation of the **1**–TEO complex implies that grinding provides the energy necessary

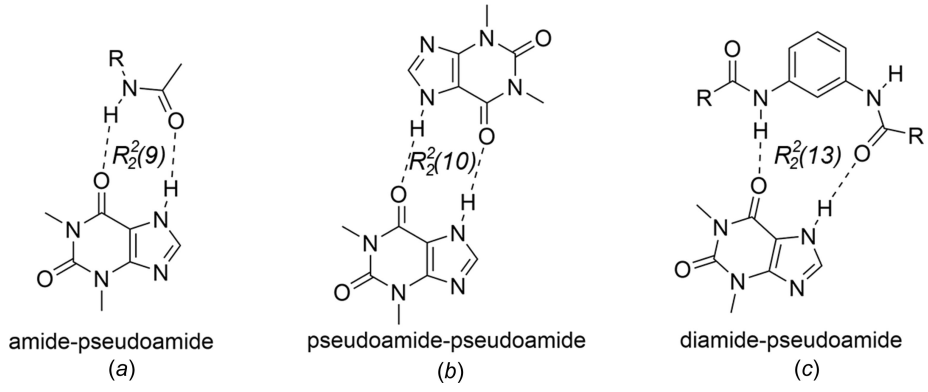

Figure 8
The observed synthons in TEO cocrystals.

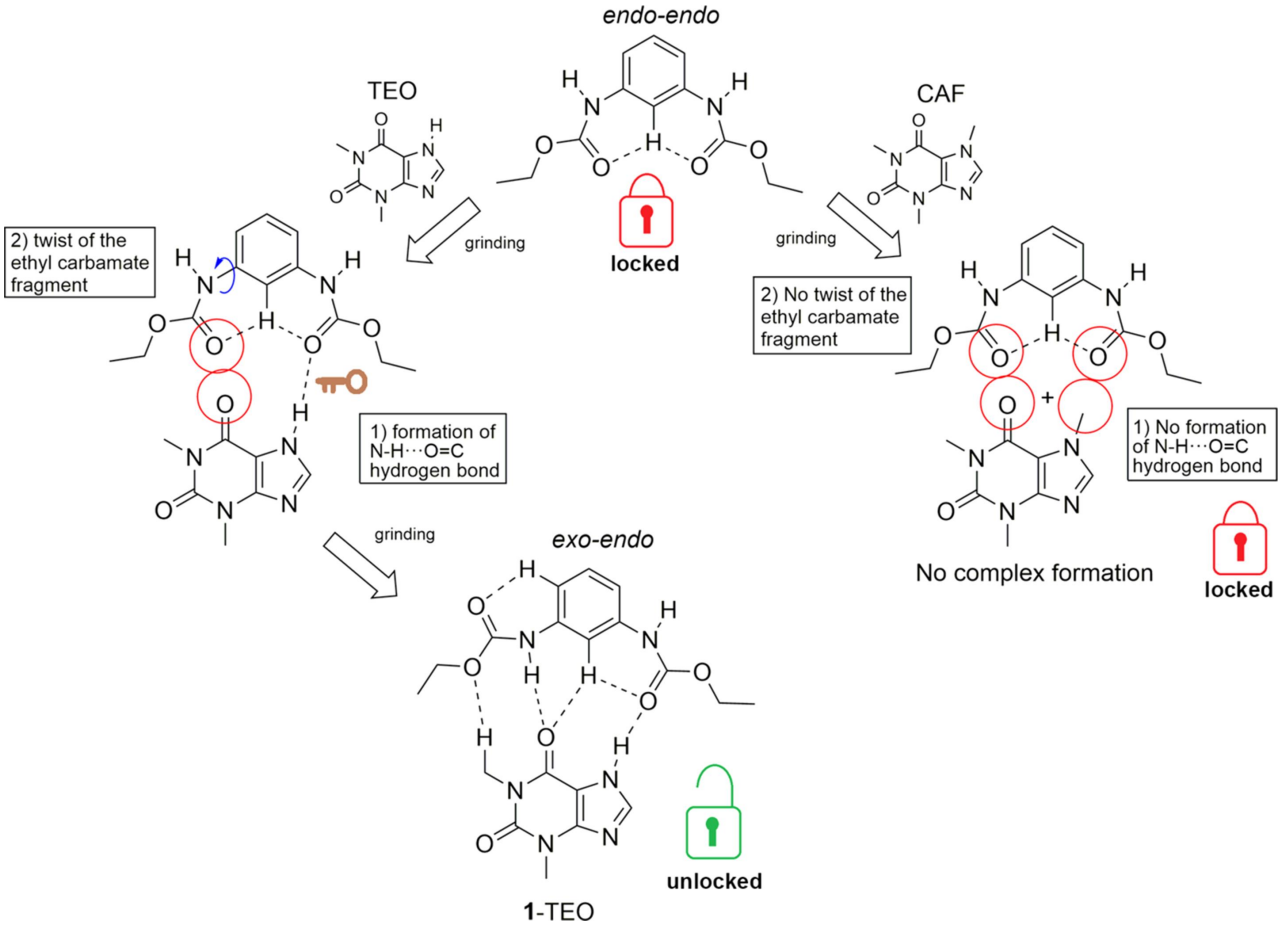

Figure 9
Conformational change of **1** in the formation of the **1**–TEO complex and the lack of conformational change of **1** in the **1**–CAF ground mixture.

for the rotation of one of the ethyl carbamate groups to adopt the *exo–endo* conformation of the 'unlocked' state (Fig. 9) [conformational change after complexation from the *exo* to the *endo* conformation (González-González *et al.*, 2014), and from the *endo* to the *exo* conformation (González-González *et al.*, 2015) is also observed in the formation of molecular complexes of diethyl *N*,*N*′-1,3-phenylenedioxalamates with 1,3-benzenediols], allowing the formation of intermolecular hydrogen bonds between **1** and TEO. On the other hand, the IR spectrum and the PXRD pattern of the **1**–CAF ground mixture indicated that the **1**–CAF complex was not formed and receptor **1** remains in the 'locked' state (*endo–endo* conformation).

To obtain information about the possible mechanism of the conformational change of **1** to form the **1**–TEO complex and the preference of receptor **1** to link TEO over CAF, firstly, the mechanochemical grinding of **1** (in the *endo–endo* form), under the same conditions to obtain the **1**–TEO complex (12 min of grinding time adding dichloromethane), was performed. The IR spectrum of **1** after 12 min of grinding time remained unchanged (Fig. S6 in the supporting information), indicating that the mechanochemical energy of the grinding is not able to drive the conformational change of free **1**. A second strategy was to perform the mechanochemical grinding of **1** and TEO without solvent to retard the formation of the complex, and compare the IR spectra of the obtained ground powder with the IR spectrum of the physical mixture and with the IR spectrum of the **1**–TEO single crystal (Fig. 10). The IR spectrum of the physical mixture showed the N—H bands at 3283 cm^{-1} for **1** and at 3119 cm^{-1} for TEO; meanwhile, the C═O bands were observed at 1704 and 1688 cm^{-1} for **1**, and at 1665 for TEO. After 3 min of 'dry' grinding, the obtained IR spectrum showed two N—H bands: a shoulder band at 3314 cm^{-1} (N—Ha) and the principal N—H band of **1** at 3287 cm^{-1} (N—Hb). The presence of two N—H bands of **1** (as in the IR spectrum of the **1**–TEO single crystal) indicates the asymmetry of the molecule by the conformational change of one of the ethyl carbamate fragments, adopting the *exo–endo* conformation. The carbonyl region showed three bands: (i) a band at 1704 cm^{-1} (C═Oa) belonging to **1**; (ii) a band at 1667 cm^{-1} (C═Ob) for TEO; and (iii) a band at 1640 cm^{-1} (C═Oc) which is present in the **1**–TEO complex. Here, the C═Ob band is slightly more intense than C═Oc, indicating that after 3 min of grinding, part of TEO remains free, and the complex has started to be formed. The IR spectra obtained after 6, 9, 12 and 15 min of 'dry' grinding showed the following: the intensity of the N—Ha band increased as a signal of the formation of the complex and the N—Hb band was red shifted; the intensity of the C═Oa band remained unchanged. As the **1**–TEO complex was formed, the intensity

of the C═Ob band of TEO at 1668 cm^{-1} decreased; meanwhile, the intensity of the C═Oc band increased. This indicates that the presence of TEO and the mechanochemical grinding induces the rotation of the ethyl carbamate group of **1** and 'unlocks' the *endo–endo* conformation to allow the formation of intermolecular interactions between **1** and TEO to form the complex (Fig. 9). The formation of the (TEO)-N—H···O═C(**1**) hydrogen-bond interaction acts as the 'key' that unlocks the *endo–endo* conformation and then the ethyl carbamate group rotates (to the 'unlocked' state) to allow the formation of the rest of the intermolecular interactions and form the diamide–pseudoamide $R_2^2(13)$ synthon in the *exo–endo* conformation (Fig. 9). On the other hand, CAF is unable to form the N—H···O═C 'key' hydrogen bond because it possesses an N—CH_3 group instead of the N—H group in TEO, avoiding the formation of the **1**–CAF complex in the same way as **1**–TEO (almost coplanar with respect to the plane of the benzene ring). It is important to mention that in the urea–CAF cocrystal and the host–guest complexes of CAF with triphenylene ketal triurea-based receptors, CAF acts as a hydrogen-bond acceptor, forming N—H···O···H—N and N—H···N···H—N hydrogen bonds where the urea group is positioned perpendicular with respect to the plane of the CAF molecule, unlike the **1**–TEO complex where **1** and TEO are coplanar (MacFhionnghaile *et al.*, 2020; Fiammengo *et al.*, 2003; Schopohl *et al.*, 2005).

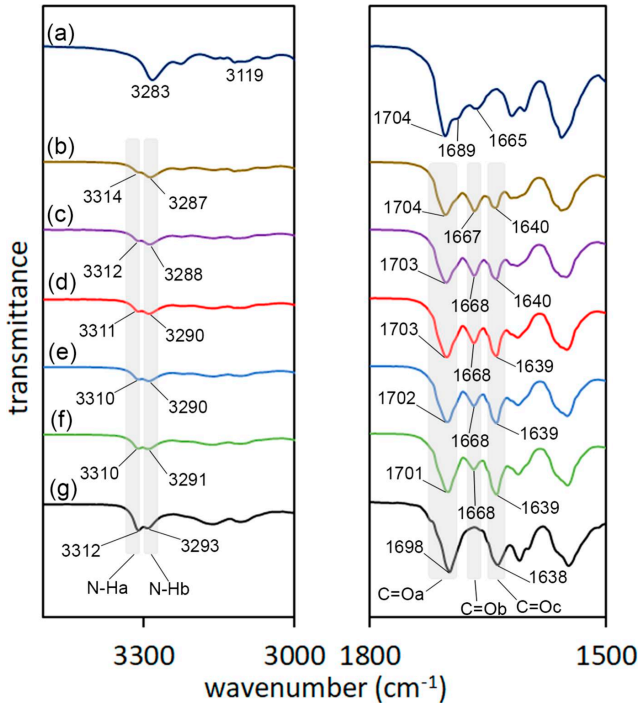

Figure 10
Partial IR spectra of (*a*) the physical mixture of **1** and TEO. Polycrystalline powder of **1**–TEO after (*b*) 3 min of grinding, (*c*) 6 min of grinding, (*d*) 9 min of grinding, (*e*) 12 min of grinding and (*f*) 15 min of grinding. (*g*) The IR spectrum of the single crystal of **1**–TEO.

4. Conclusions

The ability of receptor **1** to form host–guest complexes with TEO and CAF by mechanochemistry was evaluated, resulting only in the formation of the **1**–TEO complex involving a conformational change of **1**, in which one of the ethyl carbamate groups changes from the *endo* conformation to the *exo* conformation to allow the formation of noncovalent interactions between **1** and TEO. An IR spectroscopy study revealed that the (TEO)N—H···O═C(**1**) hydrogen bond triggers the rotation of the ethyl carbamate group from the *endo* conformation to the *exo* conformation. The formation of the **1**–CAF complex was not possible because CAF possesses an N—CH_3 group instead of the N—H group in TEO, thus avoiding the formation of the N—H···O═C hydrogen bond. The formation of **1**–TEO was evidenced by the shift of the N—H and C═O frequencies in the **1**–TEO powder complex, and by the shifts in the solid-state ^{13}C NMR signals compared with the IR and ^{13}C NMR spectra of the starting materials, suggesting the formation of N—H···O═C hydrogen bonds. The formation of the new polycrystalline phase was confirmed because the powder X-ray diffraction pattern of **1**–TEO was different from those of the starting **1** and TEO. Single-crystal X-ray diffraction analysis showed that **1** adopts the *endo–endo* conformation in the solid state and is self-assembled by N—H···O═C hydrogen bonds; meanwhile, the molecular structure of the **1**–TEO complex showed a 1:1 stoichiometric ratio, where **1** and TEO are interlinked by N—H···O═C hydrogen bonds and C—H···O interactions, and **1** adopts the *exo–endo* conformation, exhibiting the diamide–pseudomide $R_2^2(13)$ synthon. The supramolecular architecture of **1**–TEO is driven by N—H···O═C hydrogen bonds and π–π and C—H···π interactions.

Funding information

Funding for this research was provided by: Consejo Nacional de Ciencia y Tecnología (grant No. CB-2012 179674); Universidad de la Cañada (grant No. PFI-02/13); Facultad de Química, UNAM (grant No. PAIP 5000-9112).

References

AaminaNaaz, Y., Sathiyaraj, S., Kalaimani, S., Nasar, A. S. & SubbiahPandi, A. (2017). *Acta Cryst.* E**73**, 849–852.
Agilent (2013). *CrysAlis PRO*. Agilent Technologies Ltd, Yarnton, Oxfordshire, England.
Alegre-Requena, J. V., Herrera, R. P. & Díaz, D. D. (2020). *ChemPlusChem*, **85**, 2372–2375.
Ali, I., Boumoua, N., Sekkoum, K., Belboukhari, N., Ghfar, A., Ouladsmane, M. & AlJumah, B. A. (2021). *J. Chromatogr. B*, **1175**, 122738.
Angeles, E., Martínez, P., Keller, J., Martínez, R., Rubio, M. G., Ramírez, G., Castillo, R., López-Castañares, R. & Jiménez, E. (2000). *J. Mol. Struct. Theochem*, **504**, 141–170.
Baba, T., Kobayashi, A., Kawanami, Y., Inazu, K., Ishikawa, A., Echizenn, T., Murai, K., Aso, S. & Inomata, M. (2005). *Green Chem.* **7**, 159–165.
Bondy, C. R. & Loeb, S. J. (2003). *Coord. Chem. Rev.* **240**, 77–99.
Boushey, H. A. (2012). *Basic & Clinical Pharmacology*, 12th ed., edited by B. G. Katzung, S. B. Masters, A. J. Trevor, p. 345. New York: McGraw–Hill.

Colović, M. B., Krstić, D. Z., Lazarević-Pašti, T. D., Bondžić, A. M. & Vasić, V. M. (2013). *Curr. Neuropharmacol.* **11**, 315–335.
Eddleston, M. D., Arhangelskis, M., Fábián, L., Tizzard, G. J., Coles, S. J. & Jones, W. (2016). *Cryst. Growth Des.* **16**, 51–58.
Erbas-Cakmak, S., Leigh, D. A., McTernan, C. T. & Nussbaumer, A. L. (2015). *Chem. Rev.* **115**, 10081–10206.
Farrugia, L. J. (2012). *J. Appl. Cryst.* **45**, 849–854.
Fiammengo, R., Crego–Calama, M., Timmerman, P. & Reinhoudt, D. N. (2003). *Chem. A Eur. J.* **9**, 784–792.
García-Báez, E. V., López-Romero, B. A., Martínez-Martínez, F. J., Höpfl, H. & Padilla-Martínez, I. I. (2004). *Acta Cryst.* E**60**, o1488–o1490.
González-González, J. S., Martínez-Martínez, F. J., García-Báez, E. V., Cruz, A., Morín-Sánchez, L. M., Rojas-Lima, S. & Padilla-Martínez, I. I. (2014). *Cryst. Growth Des.* **14**, 628–642.
González-González, J. S., Zúñiga-Lemus, O. & Hernández-Galindo, M. C. (2017). *IOSR J. Pharm.* **7**, 28–30.
González-González, J. S., Zúñiga-Lemus, O., Martínez-Martínez, F. J., Gonzalez, J., García-Báez, E. V. & Padilla-Martínez, I. I. (2015). *J. Chem. Crystallogr.* **45**, 244–250.
Groom, C. R., Bruno, I. J., Lightfoot, M. P. & Ward, S. C. (2016). *Acta Cryst.* B**72**, 171–179.
Jiménez-Cardoso, E., Flores-Luna, A. & Pérez-Urizar, J. (2004). *Acta Trop.* **92**, 237–244.
Kim, H. J., Lee, M. H., Mutihac, L., Vicens, J. & Kim, J. S. (2012). *Chem. Soc. Rev.* **41**, 1173–1190.
Krátký, M., Štěpánková, Š., Vorčáková, K., Švarcová, M. & Vinšová, J. (2016). *Molecules*, **21**, 191.
Kubik, S. & Mungalpara, D. (2017). *Comprehensive Supramolecular Chemistry II*, edited by G. W. Gokel & J. L. Atwood, pp. 293–308. Amsterdam: Elsevier.
Larkin, P. J., Dabros, M., Sarsfield, B., Chan, E., Carriere, J. T. & Smith, B. C. (2014). *Appl. Spectrosc.* **68**, 758–776.
Lim, S. Y. K., Kuang, Y. & Ardoña, H. A. M. (2021). *Front. Chem.* **9**, 723111.
Liu, C., Dang, L., Tong, Y. & Wei, H. (2013). *Ind. Eng. Chem. Res.* **52**, 14979–14983.
Lu, Y.-Y., Yin, Q.-X., Wang, J.-K. & Zhou, L. (2005*b*). *Acta Cryst.* E**61**, o3874–o3875.
Lu, Y.-Y., Yin, Q.-X., Wang, J.-K. & Zhou, L.-N. (2005*a*). *Acta Cryst.* E**61**, o3412–o3413.
MacFhionnghaile, P., Crowley, C. M., McArdle, P. & Erxleben, A. (2020). *Cryst. Growth Des.* **20**, 736–745.
Macrae, C. F., Sovago, I., Cottrell, S. J., Galek, P. T. A., McCabe, P., Pidcock, E., Platings, M., Shields, G. P., Stevens, J. S., Towler, M. & Wood, P. A. (2020). *J. Appl. Cryst.* **53**, 226–235.
Markad, D. & Mandal, S. K. (2017). *CrystEngComm*, **19**, 7112–7124.
Matošević, A. & Bosak, A. (2020). *Arh. Hig. Rada Toksikol.* **71**, 285–299.
Mazel, V., Delplace, C., Busignies, V., Faivre, V., Tchoreloff, P. & Yagoubi, N. (2011). *Drug Dev. Ind. Pharm.* **37**, 832–840.
Mestrelab Research (2021). *Mnova Structure Elucidation*. Mestrelab Research, Santiago de Compostela, Spain.
Parsons, S., Flack, H. D. & Wagner, T. (2013). *Acta Cryst.* B**69**, 249–259.
Piper, S. L., Forsyth, C. M., Kar, M., O'Dell, L. A., Ma, J., Pringle, J. M., MacFarlane, D. R. & Matuszek, K. (2023). *Mater. Adv.* **4**, 4482–4493.
Sahoo, P. (2015). *Bioorg. Chem.* **58**, 26–47.
Santos, C. M. G. dos, McCabe, T., Watson, G. W., Kruger, P. E. & Gunnlaugsson, T. (2008). *J. Org. Chem.* **73**, 9235–9244.
Saucedo-Balderas, M. M., Delgado-Alfaro, R. A., Martínez-Martínez, F. J., Ortegón-Reyna, D., Bernabé-Pineda, M., Zúñiga-Lemus, O. & González-González, J. S. (2015). *J. Braz. Chem. Soc.* **26**, 396–402.
Schopohl, M. C., Faust, A., Mirk, D., Fröhlich, R., Kataeva, O. & Waldvogel, S. R. (2005). *Eur. J. Org. Chem.* **2005**, 2987–2999.
Shahwar, D., Tahir, M. N., Mughal, M. S., Khan, M. A. & Ahmad, N. (2009). *Acta Cryst.* E**65**, o1363.
Sheldrick, G. M. (2015*a*). *Acta Cryst.* A**71**, 3–8.
Sheldrick, G. M. (2015*b*). *Acta Cryst.* C**71**, 3–8.
Siering, C., Beermann, B. & Waldvogel, S. R. (2006). *Supramol. Chem.* **18**, 23–27.
Sun, S., Liang, N., An, H., Zhao, X., Wang, G. & Wang, Y. (2013). *Ind. Eng. Chem. Res.* **52**, 7684–7689.
Wankar, J., Kotla, N. G., Gera, S., Rasala, S., Pandit, A. & Rochev, Y. A. (2020). *Adv. Funct. Mater.* **30**, 1909049.
Webber, M. J., Appel, E. A., Meijer, E. W. & Langer, R. (2016). *Nat. Mater.* **15**, 13–26.
Yu, G. & Chen, X. (2019). *Theranostics*, **9**, 3041–3074.

supporting information

Acta Cryst. (2024). C**80**, 190-199 [https://doi.org/10.1107/S2053229624003358]

Molecular structure and selective theophylline complexation by conformational change of diethyl *N*,*N*′-(1,3-phenylene)dicarbamate

Juan Saulo González-González, Alfonso Martínez-Santos, María José Emparán-Legaspi, Armando Pineda-Contreras, Francisco Javier Martínez-Martínez, Marcos Flores-Alamo and Hector García-Ortega

Computing details

Diethyl *N*,*N*′-(1,3-phenylene)dicarbamate (1)

Crystal data

$C_{12}H_{16}N_2O_4$
M_r = 252.27
Tetragonal, $P4_12_12$
Hall symbol: P 4abw 2nw
a = 11.1312 (13) Å
c = 10.894 (3) Å
V = 1349.8 (5) Å^3
Z = 4
F(000) = 536
D_x = 1.241 Mg m^{-3}
Mo $K\alpha$ radiation, λ = 0.71073 Å
Cell parameters from 1428 reflections
θ = 4.6–26.0°
μ = 0.09 mm^{-1}
T = 298 K
Block, colourless
0.41 × 0.33 × 0.3 mm

Data collection

Agilent Xcalibur Atlas Gemini diffractometer
Graphite monochromator
Detector resolution: 10.4685 pixels mm^{-1}
ω scans
Absorption correction: analytical (CrysAlis PRO; Agilent, 2013)
T_{min} = 0.972, T_{max} = 0.976
4765 measured reflections
1620 independent reflections
1153 reflections with $I > 2\sigma(I)$
R_{int} = 0.027
θ_{max} = 29.5°, θ_{min} = 4.1°
h = −12→15
k = −12→15
l = −14→10

Refinement

Refinement on F^2
Least-squares matrix: full
$R[F^2 > 2\sigma(F^2)]$ = 0.047
$wR(F^2)$ = 0.128
S = 1.05
1620 reflections
87 parameters
0 restraints
Hydrogen site location: mixed
H atoms treated by a mixture of independent and constrained refinement
$w = 1/[\sigma^2(F_o^2) + (0.0613P)^2 + 0.124P]$ where $P = (F_o^2 + 2F_c^2)/3$
$(\Delta/\sigma)_{max}$ < 0.001
$\Delta\rho_{max}$ = 0.12 e Å^{-3}
$\Delta\rho_{min}$ = −0.14 e Å^{-3}
Absolute structure: Flack x determined using 343 quotients [(I+)-(I-)]/[(I+)+(I-)] (Parsons *et al.*, 2013)
Absolute structure parameter: −1.9 (9)

Special details

Geometry. All esds (except the esd in the dihedral angle between two l.s. planes) are estimated using the full covariance matrix. The cell esds are taken into account individually in the estimation of esds in distances, angles and torsion angles; correlations between esds in cell parameters are only used when they are defined by crystal symmetry. An approximate (isotropic) treatment of cell esds is used for estimating esds involving l.s. planes.

Fractional atomic coordinates and isotropic or equivalent isotropic displacement parameters (Å²)

	x	*y*	*z*	U_{iso}*/U_{eq}
C1	0.2786 (2)	0.3668 (2)	0.5897 (2)	0.0473 (6)
C2	0.3672 (3)	0.4536 (3)	0.5901 (3)	0.0606 (7)
H2	0.368532	0.512083	0.651112	0.073*
C3	0.4530 (3)	0.4530 (3)	0.5	0.0701 (12)
H3	0.512088	0.51209	0.5	0.084*
C6	0.2777 (2)	0.2777 (2)	0.5	0.0483 (8)
H6	0.218658	0.21866	0.5	0.058*
C8	0.0873 (2)	0.3164 (2)	0.6951 (2)	0.0495 (6)
C10	−0.0852 (3)	0.3036 (4)	0.8240 (3)	0.0832 (10)
H10A	−0.077156	0.222376	0.855168	0.1*
H10B	−0.132064	0.300798	0.749001	0.1*
C11	−0.1455 (4)	0.3789 (5)	0.9147 (4)	0.1186 (16)
H11A	−0.106482	0.370217	0.992734	0.178*
H11B	−0.227998	0.354666	0.921744	0.178*
H11C	−0.1418	0.461374	0.889143	0.178*
N7	0.1931 (2)	0.3735 (2)	0.68524 (18)	0.0584 (6)
O8	0.04488 (15)	0.24443 (16)	0.62488 (14)	0.0521 (5)
O9	0.03237 (18)	0.3535 (2)	0.79899 (17)	0.0723 (7)
H7N	0.210 (3)	0.431 (3)	0.745 (3)	0.087*

Atomic displacement parameters (Å²)

	U^{11}	U^{22}	U^{33}	U^{12}	U^{13}	U^{23}
C1	0.0505 (13)	0.0520 (14)	0.0393 (12)	−0.0004 (12)	0.0028 (11)	−0.0034 (10)
C2	0.0615 (16)	0.0584 (16)	0.0619 (15)	−0.0094 (15)	0.0074 (14)	−0.0196 (14)
C3	0.0646 (16)	0.0646 (16)	0.081 (3)	−0.022 (2)	0.0159 (18)	−0.0159 (18)
C6	0.0525 (13)	0.0525 (13)	0.0398 (16)	−0.0076 (17)	0.0061 (11)	−0.0061 (11)
C8	0.0510 (14)	0.0586 (15)	0.0389 (11)	0.0057 (13)	−0.0012 (11)	−0.0043 (12)
C10	0.068 (2)	0.102 (3)	0.079 (2)	−0.0196 (19)	0.0248 (17)	−0.0151 (19)
C11	0.096 (3)	0.137 (4)	0.123 (3)	−0.002 (3)	0.055 (3)	−0.009 (3)
N7	0.0571 (14)	0.0705 (15)	0.0475 (12)	−0.0122 (12)	0.0098 (10)	−0.0220 (11)
O8	0.0517 (10)	0.0590 (11)	0.0458 (9)	0.0001 (8)	−0.0037 (8)	−0.0117 (8)
O9	0.0630 (13)	0.0997 (16)	0.0542 (10)	−0.0190 (11)	0.0184 (9)	−0.0291 (11)

Geometric parameters (Å, º)

C1—C2	1.381 (4)	C8—O9	1.351 (3)
C1—C6	1.392 (3)	C10—O9	1.447 (4)
C1—N7	1.412 (3)	C10—C11	1.459 (5)

C2—C3	1.370 (3)	C10—H10A	0.97
C2—H2	0.93	C10—H10B	0.97
C3—H3	0.93	C11—H11A	0.96
C6—H6	0.93	C11—H11B	0.96
C8—O8	1.204 (3)	C11—H11C	0.96
C8—N7	1.343 (3)	N7—H7N	0.93 (4)

C2—C1—C6	120.4 (2)	O9—C10—H10A	109.9
C2—C1—N7	116.2 (2)	C11—C10—H10A	109.9
C6—C1—N7	123.4 (2)	O9—C10—H10B	109.9
C3—C2—C1	119.5 (3)	C11—C10—H10B	109.9
C3—C2—H2	120.3	H10A—C10—H10B	108.3
C1—C2—H2	120.3	C10—C11—H11A	109.5
C2^{i}—C3—C2	121.4 (4)	C10—C11—H11B	109.5
C2^{i}—C3—H3	119.3	H11A—C11—H11B	109.5
C2—C3—H3	119.3	C10—C11—H11C	109.5
C1—C6—C1^{i}	118.9 (3)	H11A—C11—H11C	109.5
C1—C6—H6	120.5	H11B—C11—H11C	109.5
C1^{i}—C6—H6	120.5	C8—N7—C1	128.7 (2)
O8—C8—N7	127.4 (2)	C8—N7—H7N	116 (2)
O8—C8—O9	123.9 (2)	C1—N7—H7N	115 (2)
N7—C8—O9	108.6 (2)	C8—O9—C10	116.7 (2)
O9—C10—C11	108.9 (3)		

C6—C1—C2—C3	1.3 (4)	O9—C8—N7—C1	−177.3 (3)
N7—C1—C2—C3	−179.8 (2)	C2—C1—N7—C8	166.7 (3)
C1—C2—C3—C2^{i}	−0.7 (2)	C6—C1—N7—C8	−14.5 (4)
C2—C1—C6—C1^{i}	−0.7 (2)	O8—C8—O9—C10	−1.0 (4)
N7—C1—C6—C1^{i}	−179.4 (3)	N7—C8—O9—C10	178.5 (3)
O8—C8—N7—C1	2.2 (5)	C11—C10—O9—C8	−162.4 (3)

Symmetry code: (i) $y, x, -z+1$.

Diethyl *N*,*N*′-(1,3-phenylene)dicarbamate–theophylline (1/1) (1_TEO)

Crystal data

$C_{12}H_{16}N_2O_4{\cdot}C_7H_8N_4O_2$
M_r = 432.44
Triclinic, $P\overline{1}$
Hall symbol: -P 1
a = 7.5284 (14) Å
b = 11.2362 (18) Å
c = 12.2606 (12) Å
α = 85.742 (10)°
β = 76.887 (12)°
γ = 79.803 (15)°
V = 993.5 (3) Å^3
Z = 2
F(000) = 456
D_x = 1.446 Mg m^{-3}
Mo $K\alpha$ radiation, λ = 0.71073 Å
Cell parameters from 1977 reflections
θ = 3.6–29.6°
μ = 0.11 mm^{-1}
T = 130 K
Prism, colourless
0.38 × 0.12 × 0.07 mm

Data collection

Agilent Xcalibur Atlas Gemini diffractometer
Graphite monochromator
Detector resolution: 10.4685 pixels mm^{-1}
ω scans
Absorption correction: analytical (CrysAlis PRO; Agilent, 2013)
T_{min} = 0.976, T_{max} = 0.993

11140 measured reflections
4780 independent reflections
3041 reflections with $I > 2\sigma(I)$
R_{int} = 0.051
θ_{max} = 29.7°, θ_{min} = 3.6°
$h = -10 \rightarrow 10$
$k = -15 \rightarrow 14$
$l = -16 \rightarrow 14$

Refinement

Refinement on F^2
Least-squares matrix: full
$R[F^2 > 2\sigma(F^2)]$ = 0.062
$wR(F^2)$ = 0.157
S = 1.05
4780 reflections
290 parameters
0 restraints

Hydrogen site location: mixed
H atoms treated by a mixture of independent and constrained refinement
$w = 1/[\sigma^2(F_o^2) + (0.0543P)^2 + 0.3739P]$ where $P = (F_o^2 + 2F_c^2)/3$
$(\Delta/\sigma)_{max} < 0.001$
$\Delta\rho_{max}$ = 0.29 e Å^{-3}
$\Delta\rho_{min}$ = −0.38 e Å^{-3}

Special details

Geometry. All esds (except the esd in the dihedral angle between two l.s. planes) are estimated using the full covariance matrix. The cell esds are taken into account individually in the estimation of esds in distances, angles and torsion angles; correlations between esds in cell parameters are only used when they are defined by crystal symmetry. An approximate (isotropic) treatment of cell esds is used for estimating esds involving l.s. planes.

Fractional atomic coordinates and isotropic or equivalent isotropic displacement parameters (Å^2)

	x	y	z	U_{iso}*/U_{eq}
C1	0.5463 (3)	0.2028 (2)	0.78512 (18)	0.0190 (5)
C1C	0.4338 (3)	0.2986 (2)	0.35063 (19)	0.0215 (5)
H1CA	0.353162	0.244731	0.336241	0.032*
H1CB	0.494817	0.262892	0.410779	0.032*
H1CC	0.52745	0.309502	0.282366	0.032*
C2	0.4500 (3)	0.3167 (2)	0.81742 (18)	0.0177 (5)
H2	0.410633	0.373618	0.762944	0.021*
C2C	0.2423 (3)	0.4822 (2)	0.30231 (18)	0.0201 (5)
C3	0.4111 (3)	0.3474 (2)	0.92910 (18)	0.0189 (5)
C3C	0.0487 (4)	0.6642 (2)	0.24618 (19)	0.0254 (6)
H3CA	−0.035569	0.618628	0.223344	0.038*
H3CB	0.143249	0.682163	0.18063	0.038*
H3CC	−0.021228	0.740118	0.278817	0.038*
C4	0.4733 (3)	0.2640 (2)	1.00821 (19)	0.0206 (5)
H4	0.450411	0.284584	1.084468	0.025*
C4C	0.1141 (3)	0.6329 (2)	0.43593 (17)	0.0163 (5)
C5	0.5674 (3)	0.1523 (2)	0.97481 (19)	0.0221 (6)
H5	0.607619	0.095673	1.029292	0.026*
C5C	0.1929 (3)	0.5649 (2)	0.51488 (17)	0.0173 (5)
C6	0.6062 (3)	0.1189 (2)	0.86387 (19)	0.0226 (6)
H6	0.671885	0.040927	0.842405	0.027*

C6C	0.3045 (3)	0.4509 (2)	0.49485 (18)	0.0187 (5)
C8	0.6744 (3)	0.0802 (2)	0.61652 (18)	0.0198 (5)
C8C	0.0308 (3)	0.7349 (2)	0.58082 (19)	0.0209 (5)
H8C	−0.025456	0.797994	0.631144	0.025*
C10	0.7646 (4)	−0.0096 (2)	0.44008 (19)	0.0242 (6)
H10A	0.709082	−0.082963	0.466538	0.029*
H10B	0.895855	−0.026062	0.445724	0.029*
C11	0.7503 (4)	0.0231 (2)	0.3206 (2)	0.0272 (6)
H11A	0.815312	−0.044205	0.272752	0.041*
H11B	0.806536	0.095447	0.295147	0.041*
H11C	0.619877	0.039493	0.316086	0.041*
C28	0.2235 (3)	0.5478 (2)	0.91024 (18)	0.0193 (5)
C30	0.0354 (4)	0.7401 (2)	0.92134 (19)	0.0249 (6)
H30A	−0.058581	0.717608	0.885374	0.03*
H30B	0.129797	0.772846	0.862603	0.03*
C31	−0.0537 (4)	0.8331 (2)	1.0073 (2)	0.0275 (6)
H31A	−0.114052	0.90489	0.971246	0.041*
H31B	0.040704	0.855668	1.041478	0.041*
H31C	−0.146116	0.79956	1.065306	0.041*
N1C	0.3232 (3)	0.41599 (18)	0.38423 (15)	0.0192 (4)
N3C	0.1380 (3)	0.59203 (18)	0.32969 (14)	0.0190 (5)
N7	0.5761 (3)	0.17967 (19)	0.67025 (15)	0.0200 (5)
N7C	0.1354 (3)	0.63331 (19)	0.60949 (15)	0.0211 (5)
H7C	0.162221	0.613989	0.675449	0.025*
N9C	0.0133 (3)	0.73883 (19)	0.47468 (15)	0.0203 (5)
N27	0.3066 (3)	0.45819 (18)	0.96964 (16)	0.0193 (5)
O2C	0.2650 (2)	0.44115 (16)	0.20915 (12)	0.0250 (4)
O6C	0.3800 (2)	0.38575 (15)	0.56199 (12)	0.0236 (4)
O8	0.7563 (2)	−0.00796 (16)	0.65750 (13)	0.0268 (4)
O9	0.6657 (2)	0.09231 (15)	0.50758 (12)	0.0221 (4)
O10	0.2371 (3)	0.55224 (16)	0.80905 (13)	0.0266 (4)
O29	0.1208 (2)	0.63513 (15)	0.97792 (12)	0.0217 (4)
H7	0.526 (4)	0.240 (3)	0.627 (2)	0.026*
H27	0.289 (4)	0.466 (2)	1.047 (2)	0.026*

Atomic displacement parameters (Å²)

	U^{11}	U^{22}	U^{33}	U^{12}	U^{13}	U^{23}
C1	0.0182 (13)	0.0203 (14)	0.0181 (11)	−0.0026 (11)	−0.0036 (10)	0.0007 (10)
C1C	0.0248 (14)	0.0171 (13)	0.0199 (11)	0.0051 (11)	−0.0045 (10)	−0.0036 (9)
C2	0.0193 (13)	0.0164 (13)	0.0172 (10)	−0.0010 (10)	−0.0056 (9)	0.0013 (9)
C2C	0.0195 (13)	0.0205 (14)	0.0195 (11)	−0.0022 (11)	−0.0045 (10)	0.0028 (10)
C3	0.0175 (13)	0.0185 (13)	0.0211 (11)	−0.0033 (10)	−0.0051 (10)	0.0001 (9)
C3C	0.0346 (16)	0.0207 (14)	0.0214 (12)	0.0015 (12)	−0.0128 (11)	0.0033 (10)
C4	0.0205 (13)	0.0215 (14)	0.0195 (11)	0.0010 (11)	−0.0072 (10)	−0.0011 (10)
C4C	0.0166 (12)	0.0148 (13)	0.0172 (10)	−0.0016 (10)	−0.0047 (9)	0.0017 (9)
C5	0.0208 (13)	0.0240 (14)	0.0194 (11)	0.0025 (11)	−0.0068 (10)	0.0046 (10)
C5C	0.0187 (13)	0.0174 (13)	0.0153 (10)	−0.0017 (10)	−0.0040 (9)	−0.0006 (9)

C6	0.0247 (14)	0.0188 (14)	0.0222 (11)	0.0022 (11)	−0.0057 (10)	0.0014 (10)
C6C	0.0210 (13)	0.0203 (13)	0.0148 (10)	−0.0018 (11)	−0.0055 (10)	0.0006 (9)
C8	0.0185 (13)	0.0203 (14)	0.0200 (11)	−0.0023 (11)	−0.0041 (10)	0.0003 (10)
C8C	0.0222 (13)	0.0160 (13)	0.0242 (12)	0.0002 (10)	−0.0055 (10)	−0.0054 (10)
C10	0.0258 (14)	0.0201 (14)	0.0244 (12)	0.0023 (11)	−0.0045 (11)	−0.0049 (10)
C11	0.0312 (16)	0.0233 (15)	0.0247 (12)	−0.0007 (12)	−0.0032 (11)	−0.0045 (10)
C28	0.0204 (13)	0.0184 (14)	0.0180 (11)	−0.0005 (11)	−0.0038 (10)	−0.0020 (9)
C30	0.0311 (15)	0.0197 (14)	0.0208 (11)	0.0057 (11)	−0.0083 (11)	0.0029 (10)
C31	0.0308 (16)	0.0210 (15)	0.0307 (13)	−0.0010 (12)	−0.0108 (12)	0.0031 (11)
N1C	0.0229 (11)	0.0166 (11)	0.0163 (9)	0.0012 (9)	−0.0052 (8)	0.0029 (8)
N3C	0.0232 (11)	0.0189 (11)	0.0148 (9)	0.0006 (9)	−0.0071 (8)	0.0009 (8)
N7	0.0249 (12)	0.0152 (11)	0.0165 (9)	0.0062 (9)	−0.0045 (9)	−0.0022 (8)
N7C	0.0270 (12)	0.0202 (12)	0.0174 (9)	0.0001 (9)	−0.0102 (9)	−0.0028 (8)
N9C	0.0224 (11)	0.0190 (12)	0.0192 (9)	−0.0010 (9)	−0.0063 (8)	0.0015 (8)
N27	0.0234 (11)	0.0196 (12)	0.0143 (9)	0.0020 (9)	−0.0074 (8)	0.0003 (8)
O2C	0.0345 (11)	0.0235 (10)	0.0157 (8)	0.0030 (8)	−0.0078 (7)	−0.0030 (7)
O6C	0.0300 (10)	0.0209 (10)	0.0178 (8)	0.0039 (8)	−0.0085 (7)	0.0019 (7)
O8	0.0330 (11)	0.0207 (10)	0.0224 (8)	0.0081 (8)	−0.0074 (8)	0.0006 (7)
O9	0.0269 (10)	0.0184 (10)	0.0184 (8)	0.0046 (8)	−0.0058 (7)	−0.0022 (7)
O10	0.0355 (11)	0.0242 (11)	0.0174 (8)	0.0059 (8)	−0.0086 (8)	−0.0005 (7)
O29	0.0282 (10)	0.0160 (10)	0.0189 (8)	0.0048 (8)	−0.0073 (7)	−0.0005 (7)

Geometric parameters (Å, º)

C1—C2	1.391 (3)	C6C—O6C	1.229 (3)
C1—C6	1.392 (3)	C6C—N1C	1.409 (3)
C1—N7	1.411 (3)	C8—O8	1.210 (3)
C1C—N1C	1.462 (3)	C8—O9	1.348 (3)
C1C—H1CA	0.98	C8—N7	1.352 (3)
C1C—H1CB	0.98	C8C—N9C	1.334 (3)
C1C—H1CC	0.98	C8C—N7C	1.340 (3)
C2—C3	1.390 (3)	C8C—H8C	0.95
C2—H2	0.95	C10—O9	1.452 (3)
C2C—O2C	1.228 (3)	C10—C11	1.507 (3)
C2C—N3C	1.360 (3)	C10—H10A	0.99
C2C—N1C	1.393 (3)	C10—H10B	0.99
C3—C4	1.398 (3)	C11—H11A	0.98
C3—N27	1.408 (3)	C11—H11B	0.98
C3C—N3C	1.468 (3)	C11—H11C	0.98
C3C—H3CA	0.98	C28—O10	1.219 (3)
C3C—H3CB	0.98	C28—O29	1.345 (3)
C3C—H3CC	0.98	C28—N27	1.346 (3)
C4—C5	1.369 (3)	C30—O29	1.449 (3)
C4—H4	0.95	C30—C31	1.499 (4)
C4C—N9C	1.349 (3)	C30—H30A	0.99
C4C—C5C	1.365 (3)	C30—H30B	0.99
C4C—N3C	1.376 (3)	C31—H31A	0.98
C5—C6	1.390 (3)	C31—H31B	0.98

C5—H5	0.95	C31—H31C	0.98
C5C—N7C	1.383 (3)	N7—H7	0.91 (3)
C5C—C6C	1.407 (3)	N7C—H7C	0.88
C6—H6	0.95	N27—H27	0.94 (3)

C2—C1—C6	120.5 (2)	N7C—C8C—H8C	123.3
C2—C1—N7	115.91 (19)	O9—C10—C11	107.5 (2)
C6—C1—N7	123.6 (2)	O9—C10—H10A	110.2
N1C—C1C—H1CA	109.5	C11—C10—H10A	110.2
N1C—C1C—H1CB	109.5	O9—C10—H10B	110.2
H1CA—C1C—H1CB	109.5	C11—C10—H10B	110.2
N1C—C1C—H1CC	109.5	H10A—C10—H10B	108.5
H1CA—C1C—H1CC	109.5	C10—C11—H11A	109.5
H1CB—C1C—H1CC	109.5	C10—C11—H11B	109.5
C3—C2—C1	120.2 (2)	H11A—C11—H11B	109.5
C3—C2—H2	119.9	C10—C11—H11C	109.5
C1—C2—H2	119.9	H11A—C11—H11C	109.5
O2C—C2C—N3C	122.0 (2)	H11B—C11—H11C	109.5
O2C—C2C—N1C	120.3 (2)	O10—C28—O29	123.3 (2)
N3C—C2C—N1C	117.7 (2)	O10—C28—N27	126.0 (2)
C2—C3—C4	119.4 (2)	O29—C28—N27	110.69 (18)
C2—C3—N27	123.8 (2)	O29—C30—C31	107.81 (18)
C4—C3—N27	116.7 (2)	O29—C30—H30A	110.1
N3C—C3C—H3CA	109.5	C31—C30—H30A	110.1
N3C—C3C—H3CB	109.5	O29—C30—H30B	110.1
H3CA—C3C—H3CB	109.5	C31—C30—H30B	110.1
N3C—C3C—H3CC	109.5	H30A—C30—H30B	108.5
H3CA—C3C—H3CC	109.5	C30—C31—H31A	109.5
H3CB—C3C—H3CC	109.5	C30—C31—H31B	109.5
C5—C4—C3	119.4 (2)	H31A—C31—H31B	109.5
C5—C4—H4	120.3	C30—C31—H31C	109.5
C3—C4—H4	120.3	H31A—C31—H31C	109.5
N9C—C4C—C5C	112.90 (19)	H31B—C31—H31C	109.5
N9C—C4C—N3C	125.98 (19)	C2C—N1C—C6C	126.1 (2)
C5C—C4C—N3C	121.1 (2)	C2C—N1C—C1C	115.60 (18)
C4—C5—C6	122.2 (2)	C6C—N1C—C1C	118.33 (17)
C4—C5—H5	118.9	C2C—N3C—C4C	119.69 (18)
C6—C5—H5	118.9	C2C—N3C—C3C	119.50 (19)
C4C—C5C—N7C	104.4 (2)	C4C—N3C—C3C	120.8 (2)
C4C—C5C—C6C	123.7 (2)	C8—N7—C1	127.66 (19)
N7C—C5C—C6C	132.0 (2)	C8—N7—H7	116.0 (17)
C5—C6—C1	118.2 (2)	C1—N7—H7	116.3 (17)
C5—C6—H6	120.9	C8C—N7C—C5C	106.38 (18)
C1—C6—H6	120.9	C8C—N7C—H7C	126.8
O6C—C6C—C5C	126.8 (2)	C5C—N7C—H7C	126.8
O6C—C6C—N1C	121.5 (2)	C8C—N9C—C4C	102.95 (19)
C5C—C6C—N1C	111.71 (18)	C28—N27—C3	126.79 (19)
O8—C8—O9	124.0 (2)	C28—N27—H27	118.2 (17)

O8—C8—N7	126.8 (2)	C3—N27—H27	114.9 (17)
O9—C8—N7	109.22 (19)	C8—O9—C10	114.89 (18)
N9C—C8C—N7C	113.4 (2)	C28—O29—C30	115.15 (17)
N9C—C8C—H8C	123.3		

C6—C1—C2—C3	−0.6 (4)	N1C—C2C—N3C—C4C	−0.8 (3)
N7—C1—C2—C3	178.9 (2)	O2C—C2C—N3C—C3C	0.2 (4)
C1—C2—C3—C4	1.5 (4)	N1C—C2C—N3C—C3C	−179.4 (2)
C1—C2—C3—N27	−176.7 (2)	N9C—C4C—N3C—C2C	−179.3 (2)
C2—C3—C4—C5	−1.6 (4)	C5C—C4C—N3C—C2C	−0.2 (3)
N27—C3—C4—C5	176.7 (2)	N9C—C4C—N3C—C3C	−0.8 (4)
C3—C4—C5—C6	0.9 (4)	C5C—C4C—N3C—C3C	178.3 (2)
N9C—C4C—C5C—N7C	0.5 (3)	O8—C8—N7—C1	−0.3 (4)
N3C—C4C—C5C—N7C	−178.7 (2)	O9—C8—N7—C1	178.6 (2)
N9C—C4C—C5C—C6C	−179.9 (2)	C2—C1—N7—C8	175.6 (2)
N3C—C4C—C5C—C6C	0.8 (4)	C6—C1—N7—C8	−4.9 (4)
C4—C5—C6—C1	−0.1 (4)	N9C—C8C—N7C—C5C	0.4 (3)
C2—C1—C6—C5	−0.1 (4)	C4C—C5C—N7C—C8C	−0.5 (3)
N7—C1—C6—C5	−179.6 (2)	C6C—C5C—N7C—C8C	180.0 (3)
C4C—C5C—C6C—O6C	179.6 (2)	N7C—C8C—N9C—C4C	−0.1 (3)
N7C—C5C—C6C—O6C	−1.0 (4)	C5C—C4C—N9C—C8C	−0.2 (3)
C4C—C5C—C6C—N1C	−0.4 (3)	N3C—C4C—N9C—C8C	178.9 (2)
N7C—C5C—C6C—N1C	179.1 (2)	O10—C28—N27—C3	−6.3 (4)
O2C—C2C—N1C—C6C	−178.2 (2)	O29—C28—N27—C3	173.9 (2)
N3C—C2C—N1C—C6C	1.4 (3)	C2—C3—N27—C28	2.8 (4)
O2C—C2C—N1C—C1C	0.3 (3)	C4—C3—N27—C28	−175.5 (2)
N3C—C2C—N1C—C1C	180.0 (2)	O8—C8—O9—C10	−0.4 (3)
O6C—C6C—N1C—C2C	179.3 (2)	N7—C8—O9—C10	−179.3 (2)
C5C—C6C—N1C—C2C	−0.8 (3)	C11—C10—O9—C8	−176.3 (2)
O6C—C6C—N1C—C1C	0.8 (3)	O10—C28—O29—C30	−3.8 (3)
C5C—C6C—N1C—C1C	−179.3 (2)	N27—C28—O29—C30	175.9 (2)
O2C—C2C—N3C—C4C	178.8 (2)	C31—C30—O29—C28	−173.4 (2)